Terahertz emission from the intrinsic Josephson junctions of high-symmetry thermally-managed $Bi_2Sr_2CaCu_2O_{8+\delta}$ microstrip antennas

IOP Conf. Series: Materials Science and Engineering **279** (2017) 012017 doi:10.1088/1757-899X/279/1/012017

Terahertz emission from the intrinsic Josephson junctions of high-symmetry thermally-managed $Bi_2Sr_2CaCu_2O_{8+\delta}$ microstrip antennas

Richard A. Klemm[1], Andrew E. Davis[1], Qing X. Wang[1], Takashi Yamamoto[2], Daniel P. Cerkoney[3], Candy Reid[4], Maximiliaan L. Koopman[1], Hidetoshi Minami[5], Takanari Kashiwagi[5], Joseph R. Rain[1], Constance M. Doty[1], Michael A. Sedlack[1], Manuel A. Morales[6], Chiharu Watanabe[1], Manabu Tsujimoto[1], Kaveh Delfanazari[7], and Kazuo Kadowaki[5]

[1]Department of Physics, University of Central Florida, 4111 Libra Drive, Orlando, FL 32816-2385 USA
[2]Institute for Materials Research, Hasselt University, Wetenschapspark 1 B-3590, Diepenbeek, Belguim
[3]Department of Physics and Astronomy, Rutgers University, 136 Frehlinghuysen Rd., Piscataway, NJ, 08854 USA
[4]Lockheed Martin, 5600 Sand Lake Road, Orlando, FL 32819 USA
[5]Graduate School of Pure and Applied Sciences, University of Tsukuba, 1-1-1 Tennodai, Tsukuba, Ibaraki, 305-8571 Japan
[6]Division of Health Science and Technology, Harvard Medical School, 260 Longwood Ave., Boston, MA 02115 USA
[7]Department of Physics, Cavendish Laboratory, University of Cambridge, Cambridge CB3 0HE, UK

E-mail: `richard.klemm@ucf.edu`

Abstract. We show for high-symmetry disk, square, or equilateral triangular thin microstrip antennas of any composition respectively obeying $C_{\infty v}$, C_{4v}, and C_{3v} point group symmetries, that the transverse magnetic electromagnetic cavity mode wave functions are restricted in form to those that are one-dimensional representations of those point groups. Plots of the common nodal points of the ten lowest-energy non-radiating two-dimensional representations of each of these three symmetries are presented. For comparison with symmetry-broken disk intrinsic Josephson junction microstrip antennas constructed from the highly anisotropic layered superconductor $Bi_2Sr_2CaCu_2O_{8+\delta}$ (BSCCO), we present plots of the ten lowest frequency orthonormal wave functions and of their emission power angular distributions. These results are compared with previous results for square and equilateral triangular thin microstrip antennas.

1. Introduction

Until very recently, there has been a region in the electromagnetic (EM) spectrum from about 0.1 to 10 THz over which compact coherent sources have been difficult to produce, due mainly to output power P values below 1 mW, the approximate value desired for many applications. This has been especially true in the more limited region 0.3 to 2.0 THz known as the "terahertz

gap" [1, 2]. For emission frequencies $f > 2.0$ THz, quantum cascade lasers are operational at the desired power values without cryogenic cooling [3, 4, 5]. Schottky diode frequency mixers, backward-wave oscillators, and frequency multiplier chains are operable for $f \leq 1.2$ THz [6, 7], and intracavity difference frequency generators operate over the f range of 2.6-4.2 THz [8]. Resonant tunneling diodes (RTDs) have been able to operate with sufficient power for $f < 1.4$ THz at room temperature [9, 10], but recently were shown to emit up to 2.0 THz, albeit at P values around 1 μW [11, 12].

A completely different type of source operating in the sub-THz to THz range is due to the ac Josephson effect [13, 14]. The extremely anisotropic, layered, high-transition temperature T_c superconductor $Bi_2Sr_2CaCu_2O_{8+\delta}$ (BSCCO) consists of regularly alternating superconducting and insulating layers [15, 16, 17], each of which acts as an intrinsic Josephson junction (IJJ). The best samples of BSCCO are grown by a modified traveling-solvent floating zone technique [18, 19]. When a dc voltage V is applied across the stack of N active IJJs, it gives rise to an ac current and the emission of a photon at the frequency $f = f_J = 2eV/(Nh)$ due to the ac Josephson effect, where e and h are the electronic charge and Planck's constant, respectively [13]. In addition, a BSCCO mesa structure fabricated from the top of a single crystal behaves as an electromagnetic (EM) cavity, the modes of which depend upon the geometric shape of the mesa [20]. By varying the bias V, the output f changes until it locks onto a standing wave mode of that EM cavity, resulting in coherent emission from the stack of IJJs at $f = f_c(m, n)$, where $f_c(m, n)$ is the frequency of the EM cavity mode indexed by the two integers (m, n) for the particular cavity geometry, enhancing the output power at that f value [20]-[37]. Two reviews of this phenomenon were recently published [38, 39].

However, the introduction of a dc current I into the mesa has also led to severe Joule heating problems, resulting in the formation of inhomogeneous hot spots over which the local temperature $T(\boldsymbol{r}) > T_c$ [40]-[56]. This Joule heating also caused the restrictions $V <$ 1.5 V, $f <$ 1.0 THz, and $P <$ 30μW from a single mesa [57]-[62], although a three-mesa array was reported to have a combined emission P of 0.6 mW [60].

Direct competition with the latest RTD devices [11, 12] has arisen from the construction of "stand-alone mesa sandwich structures". These are fabricated from a BSCCO mesa by cleavage from its BSCCO substrate, depositing Au films on both its top and bottom, and then sandwiching it between two insulating plates [63]-[66]. These sandwich structures allow for much more efficient Joule heat removal in the IJJ emitter devices, allowing bias V values up to 7 V and f values up to 2.4 THz, with strong emissions at particular frequencies above 1 THz [63]-[69]. Strong enhancement of the output power at particular (probably EM cavity) frequencies was also seen in a non-sandwiched rectangular stand-alone mesa and from arrays [59, 60]. Emission from mesas with slightly different heat removal designs while immersed in liquid nitrogen has also been observed [70, 71]. Hence, a more accurate name for a present device is "thermally-managed IJJ microstrip antenna (MSA)".

The important question of the sample homogeneity was raised by comparing the results of thin cylindrical (disk) conventional mesa IJJ emitters and thermally-managed IJJ disk MSAs [49, 55, 57, 65, 72]. In three conventional disk mesas, the strongest emission was observed at that of the lowest frequency transverse magnetic (1,1) disk EM cavity mode, the wave function of which has a line node passing through the disk center at a fixed angle ϕ_0. But the possible azimuthal emission anisotropy was not measured [57].

Moreover, in a more recent thermally-managed IJJ disk MSA using sapphire as the insulating plates, only very weak emission was observed at that TM(1,1) mode frequency [65]. Instead, the strongest emission was observed at about 1.0 THz, which is intermediate between the expected emission frequencies from the (0,1) and (2,1) EM cavity disk modes. As argued in the following, the disk (0,1) wave function exhibits the full rotational invariance of a one-dimensional representation (1DR) of the $C_{\infty v}$ point group appropriate for a perfectly homogeneous disk [73],

Type	Symmetry	n	n'	E	R_2	σ_x	σ_y
A_1	x^2+y^2	even	even	1	+1	+1	+1
A_2	xy	even	odd	1	+1	-1	-1
B_1	xy^2	odd	even	1	-1	+1	-1
B_2	x^2y	odd	odd	1	-1	-1	+1

Table 1. 1DR types, symmetries, allowed wave functions $\psi_{n,n'}(x,y)$ for odd or even $n, n' \geq 0$ of a rectangular microstrip antenna, and the operations of the C_{2v} point group.

and can therefore lead to an EM cavity resonance, whereas the disk TM(1,1) and TM(2,1) wave functions are two-dimensional representations (2DRs) of that point group, which would preclude the build-up of an EM cavity resonance [74, 75]. As noted above, the Au top and bottom layers also appear to amplify the emission power at the EM cavity mode frequencies [59], making the study of EM cavity mode emissions important for the development of useful devices.

2. rectangular microstrip antenna wave functions

In contrast to the three high-symmetry cases considered here, we first consider the simpler rectangular IJJ-MSA of length ℓ and width w, for which the wave (Helmholtz) equation for the magnetic vector potential $\psi \equiv A_z$ is $\boldsymbol{\nabla}^2\psi + (k')^2\psi = 0$. For the physical situation of the emission from the IJJs in BSCCO, the uniform Josephson current is in the z direction, normal to the xy plane of the rectangular MSA. The transverse magnetic (TM) boundary conditions of the electromagnetic wave equation lead to the normal derivative of the wave function vanishing on the boundary. For a rectangular MSA of any material composition with $0 \leq x \leq \ell$, $0 \leq y \leq w$, the normalized wave functions are easily found to be,

$$\psi_{n,n'}(x,y) \;=\; (2/\sqrt{\ell w})\cos(n\pi x/\ell)\cos(n'\pi y/w), \tag{1}$$

and $k'_{n,n'} = \pi\sqrt{(n/\ell)^2 + (n'/w)^2}$, where $n, n' \geq 0$, which clearly satisfy the Neumann TM boundary conditions $\frac{\partial\psi_{n,n'}(x,y)}{\partial x}\Big|_{x=0,\ell} = \frac{\partial\psi_{n,n'}(x,y)}{\partial y}\Big|_{y=0,w} = 0$. The frequencies in the vacuum radiation zone are then given by $f_{n,n'} = c_0 k'_{n,n'}/n_{\rm r}$, where c_0 is the speed of light in vacuum and $n_{\rm r}$ is the index of refraction of the MSA material. For BSSCO, $n_{\rm r} \sim 4.2$.

The wave functions for a perfect rectangular MSA are representations of the C_{2v} point group, with even or odd 180° rotational R_2 symmetry about the centroid at $(\ell/2, w/2)$ and even or odd reflections about the horizontal σ_x and vertical σ_y mirror planes, as detailed in Table 1. [73, 76]. The $n' = n = 0$ case with $f = 0$ cannot radiate. In Fig. 1, contour plots of four simplest examples of rectangular wave functions are presented. All four representations are one-dimensional representations (1DRs), as the trace of the 1×1 identity matrix E is just 1. In Fig. 1(a), $\psi(1,0)(x,y)$ is shown. It has a line node along the y axis, so it is odd (-1) about σ_y, even (+1) about σ_x, and odd (-1) under rotations (R_2) of 180° ($2\pi/2$ radians) about the centroid, so it is representation type B_1. Figure 1(b)is a contour plot of $\psi_{0,1}(x,y)$, which is odd under σ_x and R_2, but even under σ_y, so it is an example of symmetry type B_2. A contour plot of $\psi_{0,2}(xy)$ is shown in Fig. 1(c). This wave function is even under all three group operations, so it is an example of symmetry type A_1. $\psi_{1,1}(x,y)$ is pictured in Fig. 1(d). It is odd under σ_x and σ_y, and even under R_2, so it is an example of symmetry type A_2. Since any even or odd n and even or odd n' fits into this representation table, all of the rectangular MSAs are 1DRs, and can couple to the electromagnetic field, building up a resonance, and emitting with high power.

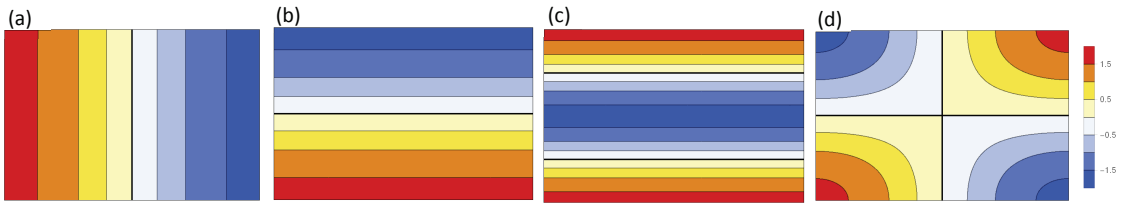

Figure 1. (colour online) Color-coded contour maps of the four simplest rectangular MSA TM wave functions and C_{2v} symmetry types: (a): (1,0), B_1; (b): (0,1), B_2; (c) (0,2), A_1; (d) (1,1), A_2. The color code applies to all four figures. The solid black lines are nodes.

Type	Symmetry	$\psi^{(\pm)}_{n,n'}(x,y)$	odd or even n	E	R_2	R_4	σ_x, σ_y	σ_{d1}, σ_{d2}
A_1	x^2+y^2	$\psi_{n,n}, \psi^{(+)}_{n,n+2p}$	e	+1	+1	+1	+1	+1
A_2	$xy(x^2-y^2)$	$\psi^{(-)}_{n,n+2p}$	o	+1	+1	+1	-1	-1
B_1	x^2-y^2	$\psi^{(-)}_{n,n+2p}$	e	+1	+1	-1	+1	-1
B_2	xy	$\psi_{n,n}, \psi^{(+)}_{n,n+2p}$	o	+1	+1	-1	-1	+1
E	fixed point nodes	$\psi^{(\theta,\pm)}_{n,n+2p+1}$	e,o	2	-1	0	0	0

Table 2. Representation types, symmetries, allowed 1DRs $\psi_{n,n}(x,y)$ and $\psi^{(\pm)}_{n,n+2p}(x,y) = [\psi_{n,n+2p}(x,y) \pm \psi_{n+2p,n}(x,y)]/\sqrt{2}$ for odd or even $n \geq 1$, 2DRs $\psi^{(\theta,+)}_{n,n+2p+1}(x,y$ of the square microstrip antenna, and operations of the C_{4v} point group. See text.

3. Square microstrip antennas

In contrast to the lower-symmetry rectangular MSA, a perfect square MSA of any material composition has much higher symmetry[73, 76, 85]. In Table 2, we list the table of the wave function symmetries under the point group C_{4v}. As noted previously[85], all 1DR wave functions given by Eq. (1) with $\ell = w$ have $|n-n'| = 2p$, where p is an integer. Hence, n and n' are either both even or both odd in 1DRs. These 1DRs have the *same* symmetry under both σ_x and σ_y, and also under both diagonal mirror planes σ_{d1} and σ_{d2}, and although they can be even or odd under rotations R_4 of $2\pi/4$ radians (90° about the centroid, they are even under R_2. These wave functions can excite cavity resonances, and the predicted radiation patterns for the ten lowest-frequency 1DR wave function modes were presented previously[85].

In contrast, wave functions $\psi_{n,n'}(x,y)$ for the square MSA for which $|n-n'| = 2p+1$, (or one of them is even and one of them is odd), are *two-dimensional representations* (2DRs). The simplest examples of these 2DR wave functions are the degenerate lowest frequency $(n,n') = (1,0)$ and (0,1), contour plots of which are pictured in Figs. 2(a) and 2(b), respectively. We note that $\psi)1,0(x,y)$ is odd under σ_y, but even under σ_x and odd under R_2. It has no symmetry under either diagonal mirror plane σ_{d1} or σ_{d2}. Similarly, $\psi_{0,1}(x,y)$ is odd under σ_x and R_2, but even under σ_y, and has no symmetry under either diagonal mirror. However, the particular orthonormal mixtures $\psi^{(\pm)}_{0,1}(x,y) = [\psi_{1,0}(x,y) \pm \psi_{0,1}(x,y)]/\sqrt{2}$ are pictured in Figs. 2(c) and 2(d). These two mixtures now have no symmetry under either σ_x or σ_y, but are still invariant under R_2. In addition, $\psi^{(+)}_{1,0}(x,y)$ pictured in Fig. 2(c) is odd under σ_{d1} (the diagonal from the upper left corner to the lower left corner), but even under the other diagonal mirror plane, σ_{d2}. Correspondingly, $\psi^{(-)}_{1,0}(x,y)$ pictured in Fig. 2(d) is even under σ_{d1}, odd under σ_{d2}, odd under

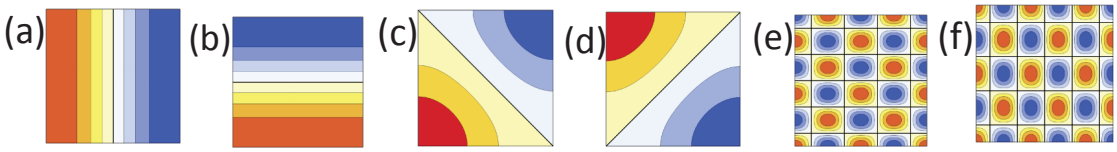

Figure 2. (colour online) Plots of the square wave functions $\psi_{n,n'}(x,y)$ for the (n,n') values (a): (1,0); (b): (0,1); (c): (1,0)+(0,1); (d): (1,0)-(0,1); (e): (4,5); and (f): (5,4).

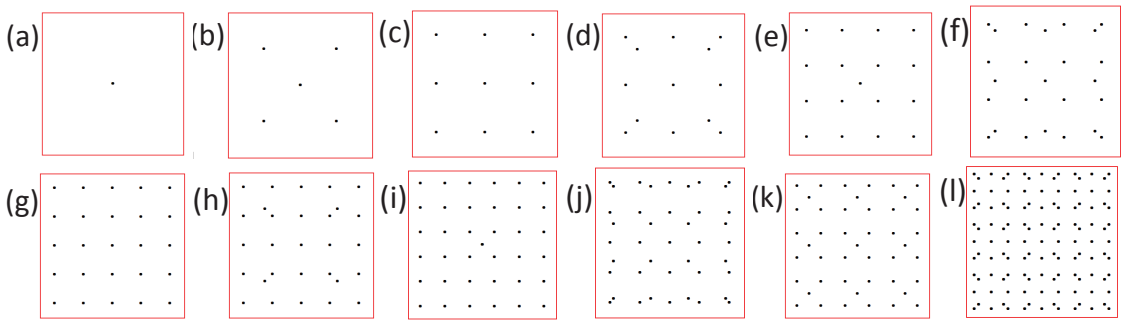

Figure 3. (colour online) Two dimensional representations of the wave functions for a perfect square MSA in order of increasing nominal frequency with (n,n') values: (a)(0,1); (b)(1,2); (c) (0,3); (d) (2,3); (e) (1,4); (f) (3,4); (g) (0,5); (h) (2,5); (i) (1,6); (j) (4,5); (k) (3,6); (l) (6,9).

R_2, and has no symmetry under either σ_x or σ_y. Moreover, we could form a general mix of these two-dimensional degenerate wave functions, forming the two-member orthonormal set

$$\psi^{(\theta,+)}_{n,n+2p+1}(x,y) = \cos\theta\psi_{n,n+2p+1}(x,y) + \sin\theta\psi_{n+2p+1,n}(x,y), \quad (2)$$

$$\psi^{(\theta,-)}_{n,n+2p+1}(x,y) = -\sin\theta\psi_{n,n+2p+1}(x,y) + \cos\theta\psi_{n+2p+1,n}(x,y). \quad (3)$$

The operations of this general pair are given by two-dimensional matrices, and identity matrix in two dimensions has the trace of 2. Thus, the functions pictured in Figs. 2(a)-2(d) could be represented by $\psi^{(\theta,+)}(1,0)$ for $n=p=0$ and respectively $\theta=\pi/2,0,\pi/4$, and $3\pi/4$. Or, they could be represented by $\psi^{(\theta,-)}(1,0)$ with $\theta=0,3\pi/2,3\pi/4$, and $\pi/4$, respectively. Thus, this is the simplest example of a 2DR wave function. Because θ could be a *random* function of the time, in an IJJ MSA, if $\theta(t)$ changes on the time scale of a single oscillation of the ac Josephson current, the form of the wave function would change, and a cavity resonance could not form. This is the main reason for this study of high-symmetry, thermally-managed IJJ MSAs. But, one might ask, what is a consistent way to represent these 2DR wave functions? One way that we have found is to consider the nodal structure that is invariant under changes in the mixing angle θ. For the (1,0) and (0,1) wave functions pictured in Figs. 2(a)-2(d), for different θ values, there is only one consistent node: the node at the centroid $(\ell/2,\ell/2)$. This nodal structure is pictured in Fig. 3(a). More generally, the ten lowest frequency nodal structures are shown in Figs 3(a)-3(j). Figure 3(j) is obtained from the two wave functions picture in Figs. 2(e) and 2(f), respectively. We note each of these nodal sets satisfies the C_{4v} group operations of the *one-dimensional* representation of type A_1, as the pattern is invariant under σ_x, σ_y, σ_{d1}, σ_{d2}, and R_4. It is further interesting to note that when (n,n') not only satisfy $n'=n+2p+1$, but also are both multiples of an odd integer, then the pattern forms a repeated pattern of the lower number indices. For example, Fig. 3(k) is the pattern for $\psi^{(\theta,\pm)}_{3,6}$, and it consists of a 3×3 array of the same pattern of $\psi^{(\theta,\pm)}_{1,2}$ pictured in Fig. 3(b). Similarly, Fig. 3(l) is the pattern for $\psi^{(\theta,\pm)}_{6,9}$,

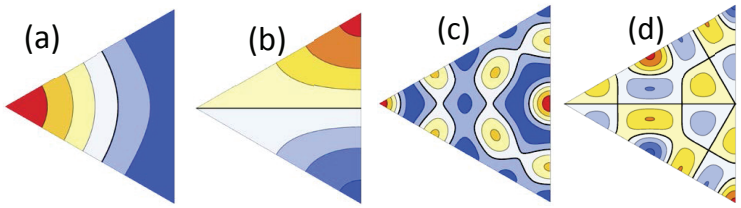

Figure 4. 2DR equilateral triangular mode examples. (a),(b) even and odd (0,1) modes. (c), (d) even and odd (4,2) modes.

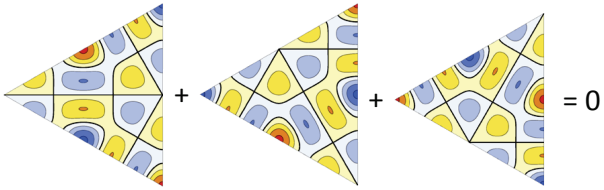

Figure 5. Pictorial summation of the (4,2) odd modes rotated by $\pm 120^\circ$ about the central axis.

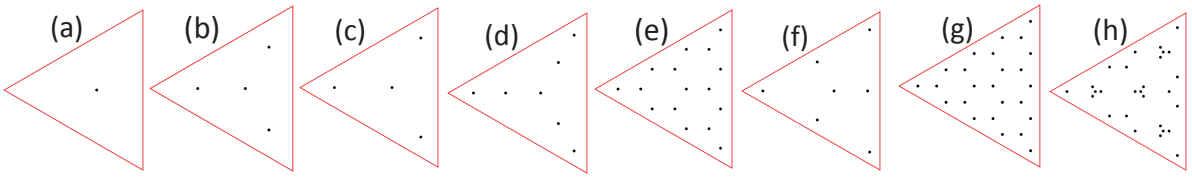

Figure 6. (colour online) Two dimensional representations of the wave functions for a perfect equilateral triangular MSA in order of increasing nominal frequency for the indicated (n, m) pairs: (a)(0,1); (b) (0,2); (c) (1,2); (d) (1,3); (e) (0,4); (f) (2,3); (g) (0,5); (h) (2,4).

which is a 3×3 array of the pattern of $\psi_{2,3}^{(\theta,\pm)}$ shown in Fig. 3(d).

4. Equilateral triangular microstrip antennas

For a perfect equilateral triangular MSA of any material composition, the wave functions are considerably more complicated than for the square[81, 85]. The wave functions for a particular symmetry plane (such as the horizontal axis that bisects an angle and the opposite side), the even wave functions that satisfy the Helmholtz equation with the Neumann (vanishing normal derivatives) boundary conditions are three products of cosine functions of x and y, respectively, and the odd functions are three products of one cosine function of x and a sine function of y[81]. The wavevectors satisfy $k'_{n,m}a = 4\pi\sqrt{n^2+m^2+nm}/(3n_{\rm r})$, where a is the length of a side of the triangle. The 1DR wave functions satisfy $|m-n| = 3p$, where p is an integer. For $p = 0$, the 1DR wave functions are non-degenerate, for for $p \neq 0$, they are double degenerate, with functions that are either even or odd about all three mirror planes normal to the planar surface and bisecting one of the angles and its opposite side. But they didn't describe the 2DR wave functions. Here we show how they can be best described.

The lowest frequency wave functions are the (0,1) modes. Those even and odd about the single symmetry plane containing the horizontal axis are pictured in Figs. 4(a) and 4(b), respectively. Similar contour plots of the even and odd (4,2) modes are shown in Figs. 4(c) and 4(d), respectively. Note that these figures only have the C_{3v} group symmetry operation of a single mirror plane, and are thus elements of a 2DR. Previously, it was shown that by forming the sum

of the wave function pictured in Fig. 2(a) with its form rotated by $\pm 120^\circ$ about the centroid, one obtains the remarkable value 0 for all points inside the triangle. In Fig. 5, we did this for the odd (4,2) wave function, just as a check on the validity of the C_{3v} group symmetry, proving that this is a 2DR wave function. More generally, the 2DR wave functions are general orthonormal sums of the two degenerate forms, such as those pictured in Figs. 4(a,b) and 4(c,d). As for the consistent method of presenting the characteristic form of such 2DR wave functions, we combine the nodal structure of these two degenerate forms, locating the set of consistent nodal points. In Fig. 8, we have done this for the eight lowest frequency 2DR wave functions. The patterns obtained from the pair pictured in Figs. 4(a,b) is shown in Fig. 6(a). It consists of a single nodal point at the centroid. The pattern obtained analogously from the (02) even and odd wave functions is shown in Fig. 6(b). Similarly, those obained from the even and odd (12), (13), (04), (23), (05), and (24) modes [the latter shown in Figs. 4(c,d)] are shown in Fig. 6(c)-6(h). In each case, the overall pattern has complete R_3 symmetry about the centroid by $\pm 120^\circ$, which is a requirement for the 1DR wave functions. This remarkable finding of the common nodal point array has not been noticed previously to our knowledge. Note that the (24) pattern pictured in Fig. 6(h) is similar to that of the (04) pattern pictured in Fig. 6(3), but four of the points in the figure have split into a triangular pattern of four points. Note that the (04) and (05) nodal patterns shown in Figs. 6(e,g) form honeycomb lattice sections commensurate with the triangle.

5. Disk microstrip antennas

For a perfect disk microstrip antenna of radius a, the wave functions $\psi \equiv A_z$ have the forms

$$\psi_{n,m}(\rho, \phi) \quad = \quad C_{n,m} J_n(k_{n,m}\rho) \cos[n(\phi - \phi_0)], \tag{4}$$

where ϕ_0 is an arbitrary angle, and the $C_{n,m}$ are normalization constants. The wave vectors $k_{n,m}$ are obtained from the Neumann boundary condition $J'_n(k_{n,m}a) = 0$, where $J'_n(z)$ is the first derivative of the regular Bessel function $J_n(z)$. In Fig. 7, contour maps of the 10 lowest frequency disk modes are shown,

We note that in Figs. 7(c) and 7(i) corresponding to the TM(01) and TM(02) cavity modes, the only nodes in the wave functions are circles centered at the origin, so these modes are rotationally invariant about the axis normal to the disk plane that passes through the disk center, and are therefore one-dimensional representations (1DRs) of point group $C_{\infty v}$[73]. The other eight modes all have one or more linear nodes that span the disk and pass through its center, and are thus not invariant under the above rotations. Hence, they are two-dimensional representations (2DRs) of point group $C_{\infty v}$, and will only be realized in imperfect devices.

We first assume that the disk MSA under study has spatial inhomogeneities that break the $C_{\infty v}$ point group symmetry. This could arise from thermal inhomogeneities, such as as hot spot that have been observed in earlier devices that were not thermally managed. In such as case, excitations of any of the cavity modes are possible, and in Fig. 8, we show three-dimensional (3D) plots of the angular distribution of the emission as predicted for BSCCO[74, 75]. In order to distinguish the 2DR wave functions from the 1DR wave functions pictorially, one should imagine that the line nodes bisecting the 2DR wave functions that pass through the origin are free to rotate about the origin, as if the ϕ_0 in Eq. (4) were a random function of the time, which would hinder the wave function from forming a resonance. Hence, the wave function would always vanish at the disk centroid, and possibly at other fixed radii, but would average to zero over a long time. Thus, these line nodes then reduce to a point at the origin (or centroid) of the disk. In Fig. 9, we have shown the reduced 2DRs that represent the 8 wave functions pictured in Fig. 7, plus the TM(13) and TM(23) modes not pictured. Note that Fig. 9(a) corresponds to all TM(n,1) modes with $n \geq 1$. For a disk of unit radius, the radii of the black circles are 0.7187 for the TM(12) mode, 0.7658 for the TM(22) mode, 0.4489 and 0.8218 for the TM(13) mode, and 0.5151 and 0.8443 for the TM(23) mode.

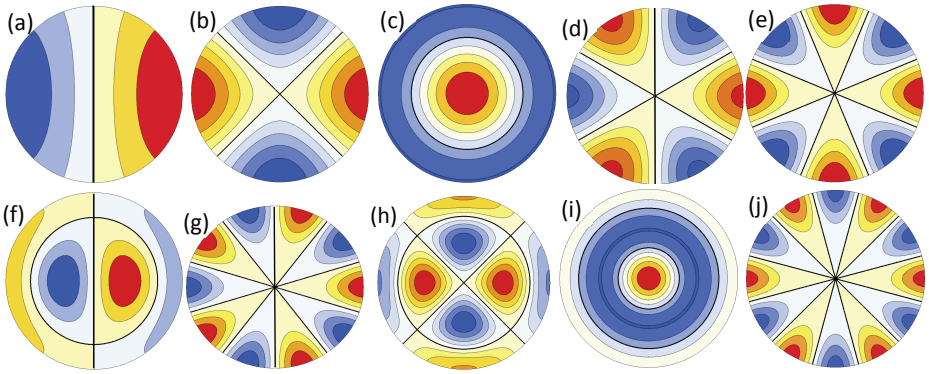

Figure 7. (colour online) Contour plots of the ten lowest frequency TM disk modes. (a) (1,1); (b) (2,1); (c) (0,1); (d) (3,1); (e) (4,1); (f) (1,2); (g) (5,1); (h) (2,2); (i) (0,2); (j) (6,1). The solid black lines and circles are nodes.

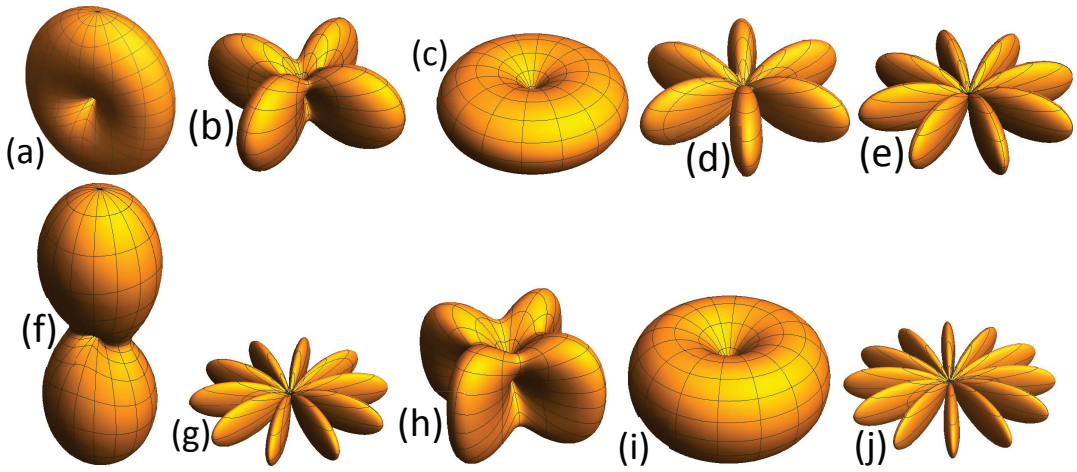

Figure 8. (colour online) Angular distribution of the predicted power distribution from the excitation of each of the ten lowest frequency EM cavity modes of an imperfect disk BSCCO device. (a)(1,1); (b) (2,1); (c) (0,1); (d) (3,1); (e) (4,1); (f) (1,2); (g) (5,1); (h) (2,2); (i) (0,2); (j) (6,1).

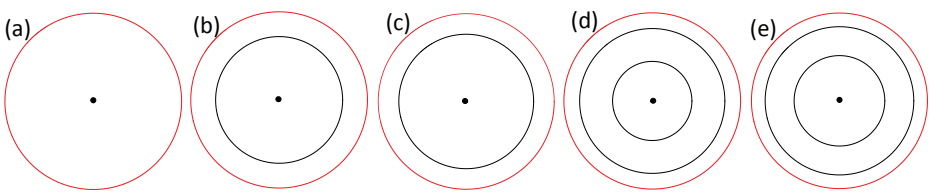

Figure 9. (colour online) Pictorial representation of the 2DR disk cavity wave functions (a)(n,1), $n \geq 1$; (b) (1,2); (c) (2,2); (d) (1,3); (e) (2,3). The red circle represents the disk edge with Neumann boundary conditions, and the black circles and central dots are nodes.

6. Conclusions

We found a set of nodal points that defines the intersection of the common nodes for the ten lowest frequency degenerate two-dimensional representations of a perfect disk, square, or equilateral triangular microstrip antenna of arbitrary composition. The positions of the nodal points are invariant under the one-dimensional operations of the respective $C_{\infty v}$, C_{4v} and C_{3v} point groups. We also presented the predicted power distributions for the ten lowest frequency cavity modes of a disk intrinsic Josephson junction microstrip antenna.

References

[1] Ferguson B and Zhang X C 2002 *Nat. Mater.* **1** 26–33
[2] Tonouchi M 2007 *Nature Photon.* **1** 97-105
[3] Walther C, Fischer M, Scalari G, Terazzi R, Hoyler N, and Faist J 2007 *Appl. Phys. Lett.* **91** 131122
[4] Fathololoumi S, Dupont E, Chan C W I, Wasilewski Z R, Laframboise F R, Ban D, Mátyás A, Jirauschek C, Hu Q, and Liu H C 2012 *Opt. Express* **20** 3866–76
[5] Kiessling J, Breunig I, Schunemann P G, Buse K, and Vodopyanov K 2013 *New J. Phys.* **15** 105014
[6] Maestrini A *et al.* 2010 *IEEE Trans. Microw. Theory Tech.* **58** (2) 1925–32
[7] Maestrini A *et al.* 2012 *IEEE Trans. THz Sci. Tech.* **2** 177–85
[8] Lu Q Y, Slivken S, Bandyopadhyay N, Bai Y, and Razeghi M 2014 *Appl. Phys. Lett.* **105** 201102
[9] Koyama Y, Sekiguchi R, and Ouchi T 2013 *Appl. Phys. Express* **6** 064102
[10] Kanaya H, Sogabe R, Maekawa T, Suzuki S, and Asada M 2014 *J. Infrared Milli. Terahz. Waves* **35** 425–31
[11] Maekawa T, Kanaya H, Asada M, and Suzuki A 2016 *Appl. Phys. Express* **9** 024101
[12] Asada M and Suzuki S 2015 *Jap. J. Appl. Phys.* **54** 020309
[13] Josephson B D 1962 *Phys. Lett.* **1** 251–53
[14] Barbara P, Cawthorne A B, Shitov S V, and Lobb C J 1999 *Phys. Rev. Lett.* **82** 1963–66
[15] Kleiner R, Steinmeyer R, Kunkel G, and Müller P 1992 *Phys. Rev. Lett.* **68** 2394–97
[16] Kleiner R and Müller P 1994 *Phys. Rev. B* **49** 1327–41
[17] Klemm R A 2012 *Layered Superconductors* vol 1 (Oxford: Oxford University Press)
[18] Mochiku T and Kadowaki K 1994 *Physica C* **235-240** 523–24
[19] Mochiku T, Hirata K, and Kadowaki K 1997*Physica C* **282-287** 475–76
[20] Ozyuzer L *et al.* 2007 *Science* **318** 1291–93
[21] Kadowaki K *et al.* 2008 *Physica C* **468** 634–39
[22] Minami H, Kakeya I, Yamaguchi H, Yamamoto T, and Kadowaki K 2009 *Appl. Phys. Lett.* **95** 232511
[23] Ozyuzer L *et al.* 2009 *Supercond. Sci. Technol.* **22** 114009
[24] Kashiwagi T *et al.* 2011 *J. Phys. Soc. Jpn.* **80** 094709
[25] Kashiwagi T *et al.* 2012 *Jap. J. Appl. Phys.* **51** 010113
[26] Benseman T M, Koshelev A E, Gray K E, Kwok W K, Welp U, Kadowaki K, Tachiki M, and Yamamoto T 2011 *Phys. Rev. B* **84** 064523
[27] Koseoglu H, Turkoglu F, Simsek Y, and Ozyuzer L 2011 *J. Supercond. Nov. Magn.* **24** 1083–86
[28] Kurter C, Ozyuzer L, Proslier T, Zasadzinski J F, Hinks D G, and Gray K E 2010 *Phys. Rev. B* **82** 224518
[29] Li M Y *et al.* 2012 *Phys. Rev. B* **86** 060505R
[30] Minami H, Tsujimoto M, Kashiwagi T, Yamamoto T, and Kadowaki K 2012 *IEICE Trans. Electron.* **E95-C** 347–54
[31] Kakeya I, Omukai Y, Yamamoto T, Kadowaki K, and Suzuki M 2012 *Appl. Phys. Lett.* **100** 242603
[32] Turkoglu F, Koseoglu H, Demirhan Y, Ozyuzer L, Preu S, Malzer S, Simsek Y, Müller T, Yamamoto T, and Kadowaki K 2012 *Supercond. Sci. Technol.* **25** 125004
[33] Yuan J *et al.* 2012 *Supercond. Sci. Technol.* **25** 075015
[34] Tsujimoto M, Minami H, Delfanazari K, Sawamura M, Nakayama R, Kitamura T, Yamamoto T, Kashiwagi T, Hattori T, and Kadowaki K 2012 *J. Appl. Phys.* **11** 123111
[35] An D Y *et al.* 2013 *Appl. Phys. Lett.* **102** 092601
[36] Kadowaki K *et al.* 2013 *Physica C* **491** 2–6
[37] Benseman T M, Koshelev A E, Kwok W K, Welp U, Vlasko-Vlasov V K, Kadowaki K, Minami H, and Watanabe C 2013 *J. Appl. Phys.* **113** 133902
[38] Welp U, Kadowaki K, and Kleiner R 2013 *Nat. Photon.* **7** 702–10
[39] Kakeya I and Wang H B 2016 *Supercond. Sci. Tech.* **29** 073001
[40] Niratisairak S, Haugen O, Johansen T H, and Ishibashi T 2008 *Physica C* **468** 442–46
[41] Wang H B, Guénon, Yuan J, Iishi A, Arisawa S, Hatano T, Yamashita T, Koelle D, and Kleiner R 2009 *Phys. Rev. Lett.* **102** 017006
[42] Wang H B *et al.* 2010 *Phys. Rev. Lett.* **105** 057002

[43] Guénon S *et al.* 2010 *Phys. Rev. B* **42** 214506
[44] Gross B *et al.* 2012 *Phys. Rev. B* **86** 094524
[45] Klemm R A, LaBerge E R, Morley D R, Kashiwagi T, Tsujimoto M, and Kadowaki K 2011 *J. Phys.: Condens. Matter* **23** 025701
[46] Minami H, Watanabe C, Sato K, Sekimoto S, Yamamoto T, Kashiwagi T, Klemm R A, and Kadowaki K 2014 *Phys. Rev. B* **89** 054503
[47] Watanabe C, Minami H, Sekimoto S, Yamamoto T, Kashiwagi T, Klemm R A, and Kadowaki K 2014 *J. Phys.: Condens. Matter*, vol. 26, 2014, Art no. 172201.
[48] Watanabe C *et al.* 2015 *Appl. Phys. Lett.* **106** 042603
[49] Watanabe C *et al.* 2016 *Supercond. Sci. Tech.* **29** 065022
[50] Krasnov V M 2011 *Phys. Rev. B* **83** 174517
[51] Yurgens A A 2011 *Phys. Rev. B* **83** 184501
[52] Tsujimoto M, Kambara H, Maeda Y, Yoshioka Y, Nakagawa Y, and Kakeya I 2014 *Phys. Rev. Applied* **2** 044016
[53] Kashiwagi T *et al.* 2014 *Appl. Phys. Lett.* **104** 022601
[54] Kashiwagi T *et al.* 2014 *Appl. Phys. Lett.* **104** 082603
[55] Demirhan Y *et al.* 2015 *Vacuum* **120** (SI) 89-94
[56] Zhou X J *et al.* 2015 *Phys. Rev. Applied* **3** 044012
[57] Tsujimoto M, Yamaki K, Deguchi K, Yamamoto T, Kashiwagi T, Minami H, Tachiki M, Kadowaki K, and Klemm R A 2010 *Phys. Rev. Lett.* **105** 037005
[58] Yamaki K, Tsujimoto M, Yamamoto T, Furukawa A, Kashiwagi T, Minami H, and Kadowaki I 2011 *Opt. Express* **19** 3193–201
[59] Tsujimoto M *et al.* 2012 *Phys. Rev. Lett.* **108** 107006
[60] Benseman T M, Gray K E, Koshelev A E, Kwok W K, Welp U, Minami H, Kadowaki K, and Yamamoto T 2013 *Appl. Phys. Lett.* **103** 022602
[61] Kitamura T *et al.* 2014 *Appl. Phys. Lett.* **105** 202603
[62] Sekimoto S, Watanabe C, Minami H, Yamamoto T, Kashiwagi T, Klemm R A, and Kadowaki K 2013 *Appl. Phys. Lett.* **103** 182601
[63] Ji M *et al.* 2014 *Appl. Phys. Lett.* **105** 122602
[64] Kashiwagi T *et al.* 2015 *Appl. Phys. Lett.* **106** 092601
[65] Kashiwagi T *et al.* 2015 *Appl. Phys. Lett.* **107** 082601
[66] Kashiwagi T *et al.* 2015 *Phys. Rev. Applied* **4** 054018
[67] Nakade K, Kashiwagi T, Saiwai Y, Minami H, Yamamoto T, Klemm R A, and Kadowaki K 2016 *Sci. Rep. (Nature)* **6** 23178
[68] Asai H and Kawabata S 2014 *Appl. Phys. Lett.* **104** 112601
[69] Rudau F *et al.* 2015 *Phys. Rev. B* **91** 104513
[70] Hao L Y *et al.* 2015 *Phys. Rev. Applied* **3** 024006
[71] Minami H, Watanabe C, Kashiwagi T, Yamamoto T, Kadowaki K, and Klemm R A 2016 *J. Phys.: Condens. Matter* **28** 025701
[72] Kadowaki K *et al.* 2010 *J. Phys. Soc. Jpn.* **79** 023703
[73] Tinkham M 1964 *Group Theory and Quantum Mechanics* (New York: McGraw-Hill)
[74] Klemm R A and Kadowaki K 2010 *J. Supercond. Novel Magn.* **23** 613–16
[75] Klemm R A and Kadowaki K 2010 *J. Phys.: Condens. Matter* **22** 375701
[76] Boas M L 2006 *Mathematical Methods in the Physical Sciences* 3rd ed. (Hoboken, NJ: Wiley)
[77] McCartin B J 2002 *Math. Probl. Eng.* **8**517–39
[78] McCartin B J 2011 *Laplacian Eigenstructure of the Equilateral Triangle*(Ruse, Bulgaria: Hikari, Ltd.)
[79] Stambaugh N and Semon M 2013 *Can. J. Phys.* **99** 1–19
[80] Klemm R A, Delfanazari K, Tsujimoto M, Kashiwagi T, Kitamura T, Yamamoto T, Sawamura M, Ishida K, Hattori T, and Kadowaki K 2013 *Physica C* **49** 30-34
[81] Cerkoney D P *et al.* 2017 *J. Phys.: Condens. Matter* **29** 015601
[82] Cerkoney D P 2015 *Terahertz radiation form high-temperature superconducting BSCCO mesas of various geometries* B. S. Honors in the Major Thesis, University of Central Florida (unpublished).
[83] Balanis C A 2005 *Antenna Theory, Analysis and Design* 3rd ed. (Hoboken: Wiley)
[84] Morales M A 2015 *Angular dependence of the emission from the intrinsic Josephson junction in pie-shaped wedge triangular BSCCO mesas* B. S. Honors in the Major Thesis, University of Central Florida (unpublished).
[85] Klemm R A, Davis A E, and Wang Q X 2017 *IEEE J. Sel. Topics Quant. Electron.* **23** 8501208
[86] Kashiwagi T *et al.* 2017 *Supercond. Sci. Tech.* **30** 074008